Pseudo-Cartesian coordinates in a model of Causal Dynamical Triangulations

Ambjorn, J.; Drogosz, Z.; Gizbert-Studnicki, J.; Gorlich, A.; Jurkiewicz, J.

Published in:
Nuclear Physics B

DOI:
10.1016/j.nuclphysb.2019.114626

Publication date:
2019

Document version
Publisher's PDF, also known as Version of record

Available online at www.sciencedirect.com

ScienceDirect

Nuclear Physics B 943 (2019) 114626

NUCLEAR PHYSICS B

www.elsevier.com/locate/nuclphysb

Pseudo-Cartesian coordinates in a model of Causal Dynamical Triangulations

J. Ambjørn [a,b], Z. Drogosz [c], J. Gizbert-Studnicki [c,*], A. Görlich [c], J. Jurkiewicz [c]

[a] *The Niels Bohr Institute, Copenhagen University, Blegdamsvej 17, DK-2100 Copenhagen Ø, Denmark*
[b] *IMAPP, Radboud University, Nijmegen, PO Box 9010, the Netherlands*
[c] *The M. Smoluchowski Institute of Physics, Jagiellonian University, Lojasiewicza 11, PL 30-348, Krakow, Poland*

Received 30 January 2019; received in revised form 12 April 2019; accepted 22 April 2019
Available online 30 April 2019
Editor: Stephan Stieberger

Abstract

Causal Dynamical Triangulations is a non-perturbative quantum gravity model, defined with a lattice cut-off. The model can be viewed as defined with a proper time but with no reference to any three-dimensional spatial background geometry. It has four phases, depending on the parameters (the coupling constants) of the model. The particularly interesting behavior is observed in the so-called de Sitter phase, where the spatial three-volume distribution as a function of proper time has a semi-classical behavior which can be obtained from an effective mini-superspace action. In the case of the three-sphere spatial topology, it has been difficult to extend the effective semi-classical description in terms of proper time and spatial three-volume to include genuine spatial coordinates, partially because of the background independence inherent in the model. However, if the spatial topology is that of a three-torus, it is possible to define a number of new observables that might serve as spatial coordinates as well as new observables related to the winding numbers of the three-dimensional torus. The present paper outlines how to define the observables, and how they can be used in numerical simulations of the model.

* Corresponding author.
E-mail addresses: ambjorn@nbi.dk (J. Ambjørn), zbigniew.drogosz@uj.edu.pl (Z. Drogosz), jakub.gizbert-studnicki@uj.edu.pl (J. Gizbert-Studnicki), andrzej.goerlich@uj.edu.pl (A. Görlich), jerzy.jurkiewicz@uj.edu.pl (J. Jurkiewicz).

https://doi.org/10.1016/j.nuclphysb.2019.114626

1. Introduction

The model of Causal Dynamical Triangulations (CDT) in four dimensions was originally formulated for systems where the spatial topology of the Universe was assumed to be spherical (S^3). In most cases the (Euclidean) proper time was assumed to be periodic with some period T. The spherical topology of the spatial part of the Universe gives a number of advantages, among which the main one is its relative simplicity. Unfortunately it also has disadvantages. In the original model the path integral includes a summation over all spatial simplicial geometries corresponding to abstract triangulations of S^3. This background independence makes it almost impossible to define reference points, except in the time direction. Another problem is caused by the numerical algorithm used in the computer simulations, which made the most interesting range in the coupling constants, i.e., the one where the phase transition lines meet, practically inaccessible. These two deficiencies may be overcome using a different choice of the spatial topology, namely the toroidal topology (T^3). In this case, the path integral defining the model will include a summation over abstract triangulations of T^3.

CDT with a toroidal spatial topology was shown to have a phase structure similar to that observed when the spatial topology was spherical [1]. We have a system with four distinct phases, where the phase transition lines are approximately the same as in the spherical case.[1] The most interesting range in the coupling constants space is now, surprisingly, fully accessible[2] and shows that the phase structure is more complicated than that conjectured earlier. Instead of a quadruple point[3] we seem to observe two triple points, connected by a phase transition line.

A finite system with a toroidal T^3 geometry can be viewed as an infinite system, where a finite elementary cell is periodically repeated infinitely many times in three directions. The resulting copies of the elementary cell may be numbered by the winding numbers. The boundary of the elementary cell is not uniquely defined. However, as we will show below, it is possible to introduce additional constraints that can make such a definition unique.

In this article we will discuss the possibility of using the set of boundaries as a reference frame that allows us to define a set of pseudo-Cartesian coordinates in the elementary cell. The spatial volume distribution associated with these coordinates can be interpreted as a distribution of $\sqrt{g(x, y, z, t)}$, which potentially permits measuring the effective action parametrized not only by a time variable but also by spatial variables. We will also define a set of new observables related to the topologically closed geodesic loops with non-trivial winding numbers.

2. Toroidal topology

Details of a formulation of the CDT model were discussed earlier in a number of articles (for a review see e.g. [2]). Let us mention here a few essential points. The basic idea is to consider the analogue of the Feynman path integral for the amplitude between two spatial states with initial and final three-geometries. It is assumed that trajectories satisfy a condition of *causality*, which means that the considered spacetimes are globally hyperbolic (permitting a global time foliation) and that the spatial topology is fixed on all leaves of the foliation. We use the Regge-type discretization of the spacetime [3]. The spacetime is constructed from elementary building

[1] Some differences may be attributed to relatively large finite size effects.

[2] The detailed analysis of this range will be the subject of an independent publication.

[3] It should be emphasized that the existence of a quadruple point was only a conjecture in the spherical case since it was located in the region of coupling constant space that was inaccessible to computer simulations.

blocks – four-dimensional simplices – with a unique length of spatial edges and a unique length of time edges. Each vertex in the system has a uniquely defined integer time parameter. As a consequence, we have two types of four-simplices: the $\{4, 1\}$-simplices (with four vertices at time t and one at $t \pm 1$) and $\{3, 2\}$-simplices (with three vertices at time t and two at $t \pm 1$). The simplices are glued together along three-dimensional *tetrahedral faces* to form a *simplicial manifold* with additional regularity constraints imposed (all simplices and sub-simplices with a particular set of vertex labels appear at most once). The existence of a global foliation means that each configuration can be analytically continued between the Lorentzian and Euclidean geometry. The Wick rotation can be interpreted as analytic continuation of the length of time links. In the Euclidean formulation the memory of the time orientation is preserved. In most cases studied the systems are assumed to be periodic in the (Euclidean) time, which means that we do not need to specify initial and final spatial geometric configurations.

For every configuration of the system we may define a dual lattice, where each simplex becomes a dual vertex and each face becomes a dual link, etc. On a dual lattice, from each vertex emerge exactly five links, corresponding to exactly five neighbors of a simplex on a direct lattice. For simplicity, we will assume that all links on a dual lattice have the same length. The basic observable to be used will be the length of a geodesic line between two simplices, i.e., the minimal number of steps (links on the dual lattice) necessary to connect the two simplices. The geodesic line is usually not unique, but the minimal distance between simplices is always well defined.

A spacetime trajectory $\mathcal{T}$ appearing in the path integral is weighted by the exponential of (minus) the Hilbert-Einstein action, which in Euclidean formulation becomes real and can be interpreted as a probability

$$\mathcal{P}(\mathcal{T}) \propto e^{-S_{\mathrm{H-E}}(\mathcal{T})}. \tag{1}$$

For a system with a finite number of simplices the action $S_{\mathrm{H-E}}(\mathcal{T})$ takes a particularly simple form[4]

$$S_{\mathrm{H-E}}(\mathcal{T}) = -(K_0 + 6\Delta)N_0 + K_4\left(N^{\{4,1\}} + N^{\{3,2\}}\right) + \Delta N^{\{4,1\}}. \tag{2}$$

In (2) the global numbers N_0, $N^{\{4,1\}}$ and $N^{\{3,2\}}$ denote correspondingly the number of vertices and the numbers of simplices of each of the two types in a triangulation $\mathcal{T}$. The dimensionless coupling constants are K_0 – related to the inverse of the gravitational constant, the cosmological constant K_4 and Δ – a function of the ratio between the time and spatial length of edges. Typically in a configuration $N_0 \propto N_4 = N^{\{4,1\}} + N^{\{3,2\}}$. Different triangulations correspond in general to different piecewise linear geometries, and the effective number of triangulations parametrized by the same set of global numbers $N^{\{4,1\}}$ and $N^{\{3,2\}}$ at K_0, Δ (i.e., with the same action) grows in the leading order as

$$\mathcal{N}(N_4; K_0, \Delta) \approx e^{K_4^{crit}(K_0,\Delta)N_4}. \tag{3}$$

As a consequence, the amplitude is defined only for $K_4 > K_4^{crit}(K_0, \Delta)$ and the limit $K_4 \to K_4^{crit}(K_0, \Delta)$ is the large-volume limit where the average number of simplices becomes large and

[4] For a piecewise linear four-dimensional geometry, defined by a four-dimensional triangulation, Regge [3] provided a simple geometric expression for the Hilbert-Einstein action, expressed in terms of link lengths and deficit angles of triangles in the triangulation. In our case, this expression simplifies further since our link lengths take only two values, corresponding to spacelike and timelike links. The end result is that the action can be expressed entirely in terms of the number of vertices N_0, the number of four-simplices $N^{\{4,1\}}$ and $N^{\{3,2\}}$, and the ratio between the length of spacelike and timelike links. See [2] for details.

where we may try to define a continuum limit. One can define similar models in 1+1 dimensions and 2+1 dimensions. Only in 1+1 dimensions can the model be solved analytically [4]. In 2+1 dimensions there exist partial analytic results [5], but to achieve a reliable understanding of the phase structure one has to rely on Monte Carlo simulations. In 3+1 dimensions Monte Carlo simulations are the only tool available [6]. In all the simulations of a 3+1 system we use a set of 7 local *moves*, which preserve topology and foliation and which are ergodic in the class of triangulations we use (see [2] for details). The Monte Carlo evolution is performed at a given set of bare couplings K_0 and Δ. The limit $K_4 \to K_4^{crit}$ is studied by considering a growing sequence of systems with volumes $\bar{N}^{\{4,1\}}$, where the volume $N^{\{4,1\}}$ is forced to fluctuate around $\bar{N}^{\{4,1\}}$. The initial configuration with a prescribed spatial topology Σ and the time extent T fixes the topology of the studied system to be $\Sigma \times T^1$. The computer program works for arbitrary spatial topology Σ and arbitrary T, so the correct choice of the initial configuration with the desired spatial topology Σ is a very important element of each simulation, although different choices with the same topology give equivalent results.

The choice of an initial toroidal spatial geometry $\Sigma = T^3$ was discussed in our earlier paper [7]. The initial configuration used to start a Monte Carlo simulation is not a minimal configuration (in the sense discussed in [7]), but it is a very convenient choice from the point of view of the present article. The configuration is based on a triangulation of a four-dimensional hypercube [8]. The topological hypercube is divided into 16 four-simplices, out of which 10 are of the $\{4, 1\}$ type and 6 of the $\{3, 2\}$ type. To build a configuration with a $T^3 \times T^1$ topology, one needs a number of hypercubes that is even and greater or equal to four. The last restriction comes from the manifold conditions: the two vertices of a link must be different. The smallest such configuration, assuming that the time period is $T = 4$, has $N_4 = 16 \cdot 4^4 = 4096$ simplices. If Σ has the topology of S^3 one can use a much smaller starting configuration.

A system with T^3 spatial topology can be viewed as an infinite system, where a finite size *elementary cell* is periodically repeated in all spatial directions (for periodic b.c. this is also the case in the time direction). The starting configuration described above corresponds to a system composed of periodically repeated triangulated four-cubes with N_4 simplices each. The definition of an elementary cell is not unique. We may additionally request that the boundary between the neighboring cells has a minimal three-volume. This condition, for a starting configuration, does not lead to a unique choice: in fact, in every spatial direction we may choose the *initial* position of a boundary in four equivalent ways, which translates into 4^3 equivalent spatial boundaries. This is a result of the relatively high symmetry of the initial configuration, which is invariant under time and spatial shifts by one unit. The exact shape of each boundary may be locally modified in such a way that it remains simply connected. This, in general, changes the three-volume of the boundary. To control the position of boundaries, we introduce in the coding of the geometry an additional information for each interface between neighboring simplices (i.e., for each dual link). In the four-dimensional case each simplex has five neighbors, as explained above. For each dual link we introduce the integer-valued spatial vector $\vec{v}$, with entries having values $\pm 1,\ 0$ in each spatial direction. Value 0 corresponds to the case where both the simplex and a particular neighbor are in the same elementary cell. Values ± 1 mean that crossing the interface we enter the neighboring elementary cell in the positive or the negative direction. For the initial configuration choice we assign values to the vector field $\vec{v}$ for all interfaces between neighboring simplices. In any given configuration, we may form a sum of vector fields along any loop joining the simplices on a dual lattice. For a trivial closed loop the sum must be a zero vector. For a non-trivial closed loop (closed by periodic b.c.) the sum gives topological information about the loop's winding number.

In the numerical simulations the standard algorithm is using a finite set of local *moves*. Each move affects only a finite part of the configuration (i.e., of the triangulation), keeping the rest unchanged. Since Hilbert-Einstein action (2) does not depend on the position of the boundaries, the decision to accept (or reject) the move does not depend on a position of the boundaries. The position of the boundaries will however play an important role in the construction proposed in this paper. Therefore, before the move is performed we check if the boundaries between elementary cells pass through the affected region of the configuration. If this is not the case, the move is performed using the standard Monte Carlo algorithm. If, however, a boundary between two cells crosses the part of the triangulation where the geometry of connections between simplices is to be changed, then we modify locally the position of the boundary. The modification is done in such a way that the boundary remains connected, but is deformed so as to lay wholly outside of the region of the triangulation that is going to be affected by the move. Such a modification can always be done and does not change the action, but in general it will increase the size of the boundary. The move can now be performed in a standard way. After the move, we check if a simple local modification of the boundary can reduce its size (its three-volume). If this is the case, the modification of the position of the boundary is made. From time to time, we perform an additional check, independent of the moves, whether a local modification of any part of the boundaries can minimize their volumes. If so, then such a modification is always accepted.

All measurements described in this article were performed for the toroidal spatial topology in the de Sitter phase (the so-called C phase) at a special point in the parameter space $K_0 = 2.2$ and $\Delta = 0.6$ for systems with $T = 4$ and a sequence of volumes $N^{\{4,1\}}$. The same point in the parameter space was earlier analyzed in simulations of systems where the configurations had spherical spatial topology [6], as well as in systems with configurations of toroidal spatial topology [7].

3. Pseudo-Cartesian coordinates

A given set of boundaries can be used to define what we will denote as the *pseudo-Cartesian coordinates*. The procedure is as follows:

- We start from a boundary,[5] say, orthogonal to the direction $\mathbf{x}$, and we mark all simplices adjacent to the boundary in the direction we define to be *positive* as having the coordinate $\mathbf{x} = 1$.
- We move (on the dual lattice) in the positive direction to the second layer of simplices at a unit distance from the first layer. We mark these simplices as having a coordinate $\mathbf{x} = 2$.
- We continue the same process until all simplices in the system are marked, and a maximal extent in the x direction is reached.
- The same procedure can be started from the layer of simplices adjacent to a boundary in the *negative* direction. The simplices in that layer are marked as having a coordinate $\mathbf{x}' = 1$.
- We continue the process as before.
- This way each simplex is assigned the values of the coordinates $\mathbf{x}$ and $\mathbf{x}'$.
- Exactly the same method can be used to define the coordinates $\mathbf{y}$, $\mathbf{y}'$, $\mathbf{z}$ and $\mathbf{z}'$.

For a (two-dimensional) visualization of the procedure please refer to Fig. 1.

[5] The boundaries are labeled x, y and z, based on their positions in the initial configuration, which is related to the hypercube.

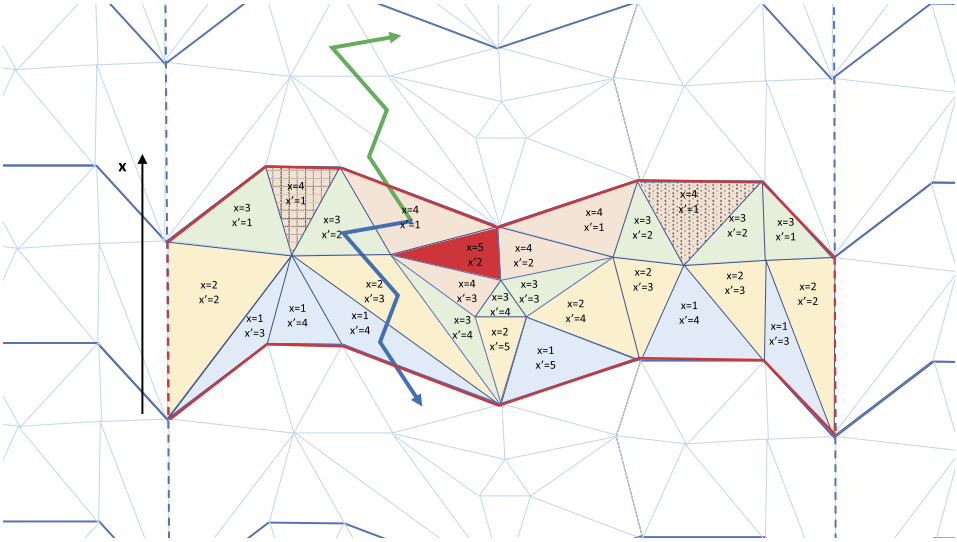

Fig. 1. The (two dimensional) visualization of a triangulation (colored triangles) with toroidal topology. The (smallest) boundary orthogonal to the $\mathbf{x}$ direction is plotted as a red solid line, and the boundary orthogonal to the other direction as a red dashed line (the red solid lines, as well as the red dashed lines, are identified). Different colors mark different $\mathbf{x}$ coordinates. All triangles of the same color and texture form single *slices* (see Section 4 for description): for $\mathbf{x} = 1, 2, 3, 5$ one has only a single slice for each $\mathbf{x}$ coordinate, but for $\mathbf{x} = 4$ one can distinguish three separate slices. All triangles, but the dark red one, belong to the *trunk*, and the dark red triangle belongs to the *branch* (see Section 4 for description). Alternatively (see Section 5), one can treat the toroidal triangulation as an elementary cell which periodically repeats in each direction (blank triangles). For each triangle one can find (one or more) minimal loops with a nontrivial winding number: all triangles whose centers are marked by a solid zigzag arrow belong to the same $\{1, 0\}$ loop (green arrow), and also to the same $\{-1, 0\}$ loop (blue arrow), the length of these loops is 4. One can construct similar loops for all other triangles and measure their length. One can also construct the minimal loops with other winding numbers in all directions. (For interpretation of the colors in the figure(s), the reader is referred to the web version of this article.)

One should note that although each three-dimensional boundary is simply connected, this does not need to be the case for three-dimensional surfaces separating $\mathbf{x}$ and $\mathbf{x}+1$ layers. The set of numbers $\{\mathbf{x},\ \mathbf{x}'\}$ represents the distance of a simplex to a boundary, i.e., the number of links on the dual lattice, in negative and positive directions.

The first question one may ask is if the definition of a boundary between elementary cells, as implemented by the minimization procedure, is unique. For the simple initial configuration described above this is definitely not the case. As already explained, in each spatial direction we may choose the initial position of a boundary between the copies of the elementary cell in four equivalent ways, giving rise to 4^3 equivalent (minimal) boundaries. Since the updates of geometry do not "feel" the position of the boundaries, we can run a parallel simulation, where the evolution of geometry is exactly the same, but the initial choice of a position of a boundary is different. In this way, during the thermalization process, each simplex can be assigned its coordinates using the two different positions of a boundary. Comparing the two coordinates, say $\mathbf{x}$ and $\tilde{\mathbf{x}}$, we define the difference between the two alternative definitions by measuring the ratio M of the number of simplices for which $\mathbf{x} = \tilde{\mathbf{x}}$ to the total number of simplices. This quantity is initially zero. A value $M = 1$ means that two definitions become equivalent, or in other words, that the two boundaries fully overlap. Analogous quantities can be defined in $\mathbf{y}$ and $\mathbf{z}$ directions. In the Fig. 2 we present the evolution of the parameter M for three directions in a system with

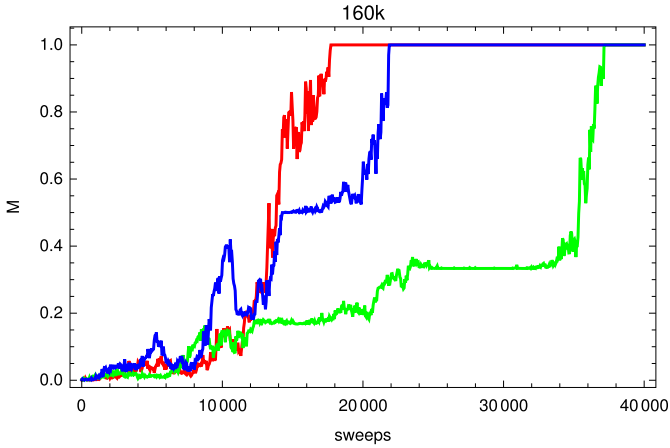

Fig. 2. The example of the evolution in computer time of the boundary merging ratio M in all three directions (**x** red line, **y** green line, **z** blue line) for a system with a volume $N^{\{4,1\}}$ =160k. The two initial choices of the position of boundaries are the most distant in each direction.

$N^{\{4,1\}}$ =160k. The initial position of boundaries was chosen as the most distant permitted by the symmetry of the starting configuration. Similar experiments were repeated for other initial choices of boundaries and other system sizes. In all cases the result was the same, indicating that the algorithm used is powerful enough to find a global minimum of the boundary size in all directions. It is a non-trivial result, because naïvely one may expect the existence of a complicated landscape of local minima. This also means that we do not have to worry about the initial choice of the position of boundaries.

Since the considered systems are periodic in (Euclidean) time with a period T, each simplex can be assigned a coordinate **t**. The layer with $\mathbf{t} = 1$ is chosen as the set of $\{4, 1\}$-simplices with four vertices at $t = 1$. We follow the same prescription as before, for instance $\mathbf{t} = 2$ is composed of a set of $\{3, 2\}$-simplices at a unit distance from the $\mathbf{t} = 1$ in the *positive* time direction. We continue until we reach the layer $\mathbf{t} = 4T$ formed from $\{1, 4\}$ simplices. We could define coordinates $\mathbf{t}'$ similarly as before, but for the time direction for each system we have a trivial relation $\mathbf{t} + \mathbf{t}' = 4T + 1$, resulting from the trivial periodicity by construction in the time direction.

In the spatial directions a similar relation is not satisfied and the distribution of values for, say, **x** and $\mathbf{x}'$ is non-trivial. Below, in the Fig. 3, we present the probability distribution $P(\mathbf{x}, \mathbf{x}')$ to find a simplex with given values of coordinates **x** and $\mathbf{x}'$ in a system with $N^{\{4,1\}}$ =160k. The distribution is constructed by averaging over 800 statistically independent configurations and summed over all simplices in the system.

Distributions of this type contain interesting information about geometric properties of the system in spatial directions. We should remember that simplices with coordinates $\mathbf{x} = 1$ and $\mathbf{x}' = 1$ lie on a *minimal* boundary between elementary cells. Such a boundary separates regions where gravitational fluctuations produce volume concentrations. Qualitatively, in the small **x** and $\mathbf{x}'$ regions the volume of the system is suppressed. A special role is played by the distribution $p(L_x)$ of the quantity $L_x = \mathbf{x} + \mathbf{x}'$ (and similar quantities L_y and L_z). Although for the initial configuration the shape of the elementary cell is symmetric with respect to the exchange of directions **x**, **y** and **z**, during the thermalization process the shape of the elementary cell may be deformed. In fact, we expect that the distributions $p(L_x)$, $p(L_y)$ and $p(L_z)$ should overlap, up to a finite shift in L_i. This is indeed the case. In the Fig. 4 we show the distributions $p(\mathbf{x} + \mathbf{x}')$,

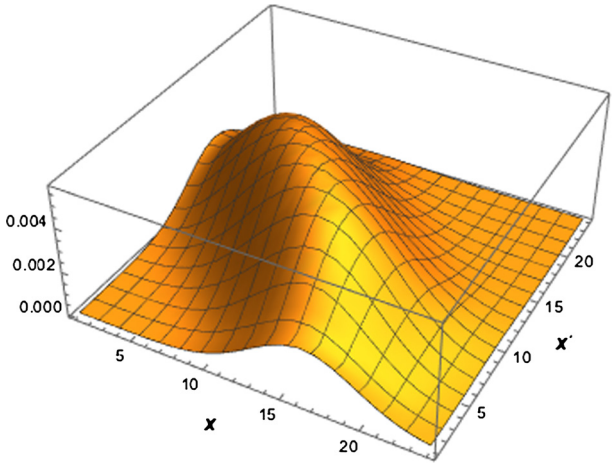

Fig. 3. The distribution $P(\mathbf{x}, \mathbf{x}')$ for a system with $N^{\{4,1\}} = 160$k.

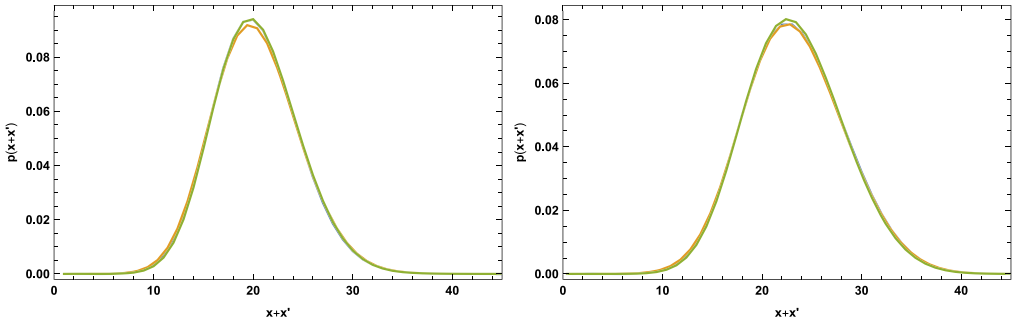

Fig. 4. Distributions of $p(\mathbf{x}+\mathbf{x}')$ (blue), $p(\mathbf{y}+\mathbf{y}')$ (green) and $p(\mathbf{z}+\mathbf{z}')$ (orange) for systems with $N^{\{4,1\}} = 80$k (left) and $N^{\{4,1\}} = 160$k (right).

$p(\mathbf{y}+\mathbf{y}')$ and $p(\mathbf{z}+\mathbf{z}')$ for systems with $N^{\{4,1\}} = 80$k and $N^{\{4,1\}} = 160$k. In both cases a complete overlap is achieved by applying shifts of order one.

Comparing the two plots we realize that the shape of distributions seems to be the same, up to a scaling, depending on the total volume. In the Fig. 5 we compare the two volumes ($N^{\{4,1\}} = 80$k and 160k), applying a scaling factor $1/2^{1/4}$ to the distribution for a larger system. This agrees with the expected scaling, if we assume that the Hausdorff dimension in de Sitter phase is $d_H = 4$.

Another important information about the shape of the volume distribution in spatial directions is hidden in the distribution $p(\mathbf{x}-\mathbf{x}')$ of the difference between $\mathbf{x}$ and $\mathbf{x}'$. For a toroidal topology one expects this distribution to be approximately constant, as was already observed in [7] for a similar distribution in time t. While the periodicity in time was exact, the period in the spatial directions, say the $\mathbf{x}$ direction, will vary, depending on $L_x = \mathbf{x} + \mathbf{x}'$. As a consequence, we break the spatial translational symmetry and force the system to have the smallest volume at the small $\mathbf{x}$ limit. In the central range of the plot, where $\mathbf{x} \approx \mathbf{x}'$ we expect the distributions to be approximately flat, constant in the infinite volume limit. Below, in the Fig. 6, we show the amplified dependence of the volume distribution $P(\mathbf{x}, \mathbf{x}')$ as a function of the re-scaled variable $\frac{1}{2}(\mathbf{x}-\mathbf{x}')/(\mathbf{x}+\mathbf{x}')$ for a range of values of $15 \leq \mathbf{x}+\mathbf{x}' \leq 30$ for a system with $N^{\{4,1\}} = 160$k.

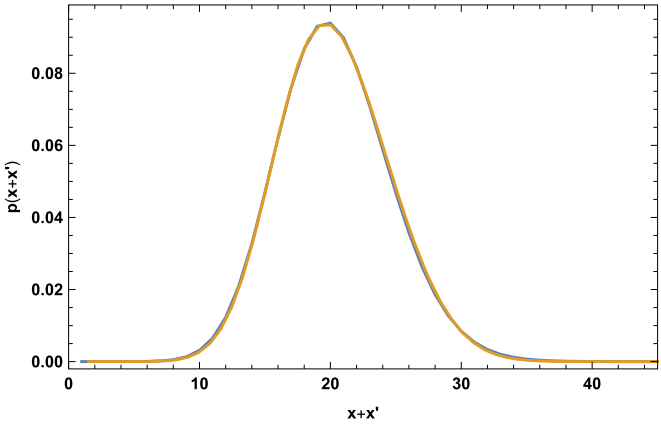

Fig. 5. The scaling of a distribution $p(\mathbf{x}+\mathbf{x}')$ for two system sizes ($N^{\{4,1\}}$ =80k and 160k, colored blue and orange, respectively). For the larger system the distribution is rescaled by a factor $1/2^{1/4}$.

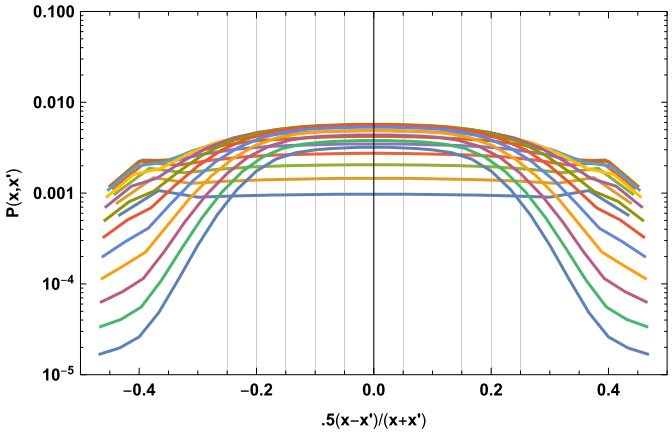

Fig. 6. Central part of the distribution $P(\mathbf{x},\mathbf{x}')$ as a function of the re-scaled variable $\frac{1}{2}(\mathbf{x}-\mathbf{x}')/(\mathbf{x}+\mathbf{x}')$. The curves correspond to the increasing values of $\mathbf{x}+\mathbf{x}'$ in a sequence of colors: blue, orange, green etc.

We see that the distributions are indeed approximately flat in the central range. The large volume limit can be extrapolated by comparing distributions of $p(\mathbf{x}-\mathbf{x}')$ for systems with volumes 80k and 160k. We see that for a larger system the distribution gets wider (Fig. 7).

4. The fractal structure of equal x layers

As explained above, the constant $\mathbf{x}$ layer is by construction connected for $\mathbf{x}=1$. We will study the geometric structure of layers with higher values of $\mathbf{x}$. To do this we define the concept of a *slice*. The idea is very similar to that used in 2d Euclidean Dynamical Triangulations. The construction is based on following the front of a diffusion wave on the dual lattice. We start at a randomly chosen simplex with spatial coordinate $\mathbf{x}$ and constrain the diffusion process to take place in the subset of simplices with spatial coordinate $\tilde{\mathbf{x}} \geq \mathbf{x}$, i.e., in the bounded part of the given triangulation lying in between the set of simplices with coordinate $\mathbf{x}-1$ and the boundary

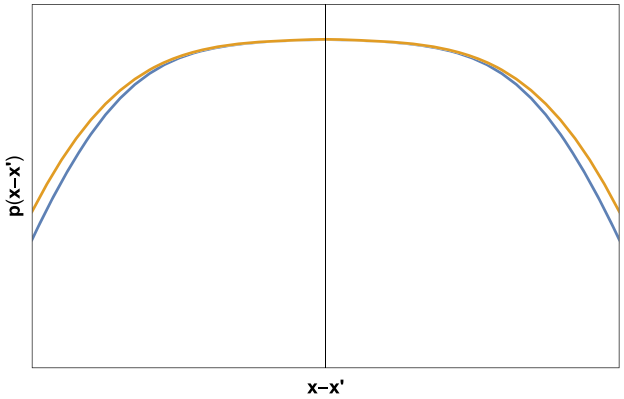

Fig. 7. The integrated distribution $p(\mathbf{x}-\mathbf{x}')$ as a function of $\mathbf{x}-\mathbf{x}'$ for volumes $N^{\{4,1\}}$ =80k (blue) and 160k (orange).

of the elementary cell. In each diffusion step we mark simplices we meet on the way. The marked simplices form a new limiting layer for the next step.

If the geometry of the manifold were trivial, in such a process we could reach all simplices in the bounded region of the configuration described above. The fractal nature of geometry means that, in general, only a part of the bounded region is reached. Completing the process we find a set of simplices with the same coordinate $\mathbf{x}$ as the initial simplex. The set of these simplices forms a *slice*. All simplices belonging to the slice can be joined by at least one path lying in the bounded region. Repeating the same process starting at a different simplex with a coordinate $\mathbf{x}$, we either end with the same slice or produce a different slice, disconnected from the previous one. The set of simplices reached from the set belonging to a common slice has a tree-like structure, where the slice plays a role of the root.

The procedure is performed repeatedly, assigning in this way a slice index to all simplices of the configuration:

- The first slice consists of all simplices with $\mathbf{x} = 1$.
- In the layer with $\mathbf{x} = 2$ we find all simplices that can be connected by a path that does not cross the elementary cell boundary and never goes below $\mathbf{x} = 2$.
- We find all separate slices for $\mathbf{x} = 2$.
- We repeat the same procedure for $\mathbf{x} = 3$. In this case, we restrict the class of paths not to go below $\mathbf{x} = 3$.
- We continue until all slices are found.

For a (two-dimensional) visualization of the procedure please refer to Fig. 1.

By construction, each slice (except the first one) has exactly one parent slice, and it may have a larger number of children (or no children at all). Following the sequence of connected slices with an increasing value of $\mathbf{x}$, we may either reach the boundary or end in a blind alley. In the first case we say that the sequence belongs to the *trunk*, in the second case it belongs to a *branch*. The structure looks like a tree, with the trunk connecting the lower and upper boundaries. The trunk may split into several outgrowths. The branches emerge from the trunk slices and, by definition, never reach the boundary of the elementary cell. We would like to interpret the branches as the effect of quantum fluctuations and the trunk as a semi-classical background.

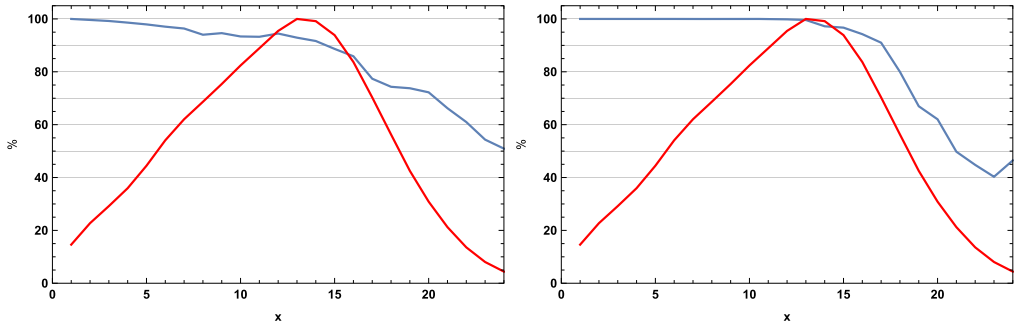

Fig. 8. The fraction of the trunk volume in the total volume (left) and of the largest slice volume in the trunk volume (right). The (normalized) total volume distribution is drawn in red.

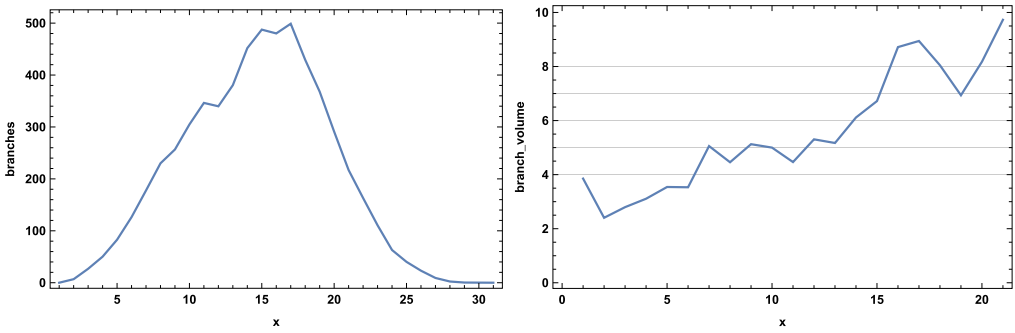

Fig. 9. The number of branches at a distance **x** (left) and the average branch volume (right).

Below we illustrate the properties of the trunk-branch construction for one particular well-thermalized configuration in the de Sitter phase. The configuration was obtained for a system with $K_0 = 2.2$, $\Delta = 0.6$, $T = 4$ and the total number of simplices $N_4 = 370\,724$. At each value of the coordinate **x** we split the volume into the part belonging to the trunk and the part belonging to branches. In the Fig. 8 we show the fraction (percent) of volume in the trunk, relative to the total volume at a coordinate **x**, and the fraction of volume of the largest slice, relative to the trunk volume at the same coordinate **x**. In the same plot (in red) we show the total volume distribution as a function of **x**. The distribution is normalized to reach 100% at its maximum. The distribution in the plot (as compared to that in the Fig. 3) can be viewed as a projection of volume on the **x** axis. In the plot all distributions are averaged over directions **x**, $\mathbf{x}'$, **y**, $\mathbf{y}'$, **z** and $\mathbf{z}'$.

As can be seen, for a configuration in the de Sitter phase, the trunk contains the biggest part of volume and the largest slice captures almost all trunk volume up to the value of **x** where the volume is maximal (recall that by construction the volume as a function of **x** is small near the boundaries).

In the next plot, Fig. 9, we show the average number of branches at a distance **x** and the average volume per branch. As can be seen, the number of branch slices grows together with volume, but the average volume per branch slice is relatively small. The maximal length of a branch, defined as a number of steps between the consecutive slices along the branch necessary to reach the trunk slice from a branch slice, is six, which means that branches are rather short.

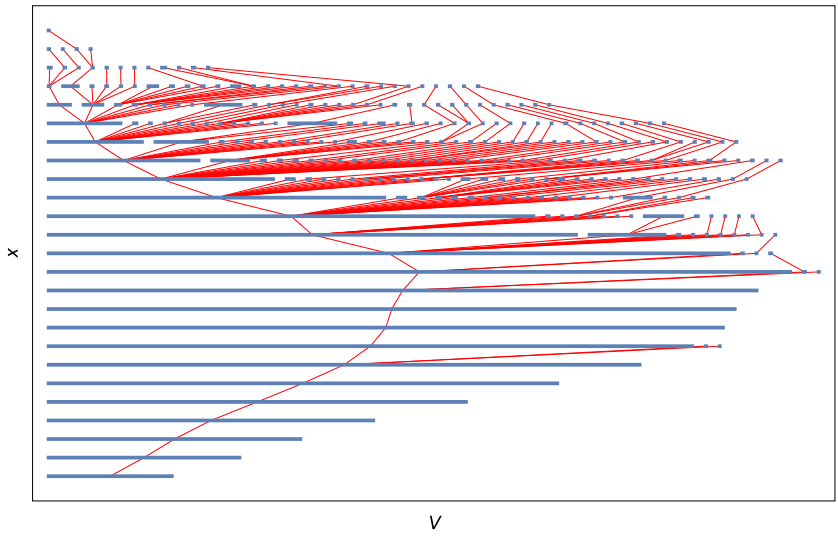

Fig. 10. The tree structure of the branching for the increasing value of a coordinate **x**. For clarity each slice is represented as a line with the length proportional to its volume. The red lines connect the centers of the consecutive slices.

The tree structure representing the branching of slices with the increasing value of a coordinate **x** is presented in the Fig. 10. For clarity the plot contains only the slices belonging to the trunk. The volume of slices is shown as the horizontal length of the line.

5. Loops with a non-trivial winding number

In the former section we analyzed the fractal structure of an elementary cell, parametrized by what we denoted as pseudo-Cartesian coordinates. Using the same elementary cell and its periodic extensions to neighboring cells, we will now introduce a set of new topological observables, which measure the geodesic distance between a simplex and its copy in the neighboring cells in different spatial directions. Like before, the measurement is performed by following paths defined by the front of a diffusion wave, starting from a given simplex, but in this case we consider the torus as an infinite system where simplices reached after r diffusion steps are labeled by the (unique) index in the elementary cell and also by the number of times a path crossed the boundaries. If one finds a simplex with the same cell index and nontrivial number of crossings, say, $\{m_1,\ m_2,\ m_3,\ m_4\}$, it means that there exists at least one topologically closed geodesic line characterized by these winding numbers, namely the shortest such path.[6] In general there are many paths with the same length, but for a particular simplex and particular values $\{m_1,\ m_2,\ m_3,\ m_4\}$ there is always the shortest distance, characterizing these two copies of a simplex. In a $4D$ system the number of elementary cells at a large distance R is expected to grow as R^3. As a consequence, measuring the complete distribution of paths up to some length

[6] The "shortest" is meant in a graph-theoretical sense: we follow a link path (on the dual lattice) and the length is the number of links. This is not necessarily the shortest path if we consider our triangulation as a piecewise linear manifold. However, we do not expect this difference to be important when we discuss generic fractal properties, like the Hausdorff dimension of a generic triangulation in the limit of infinitely large triangulations. By an abuse of language we still call the shortest link path a geodesic.

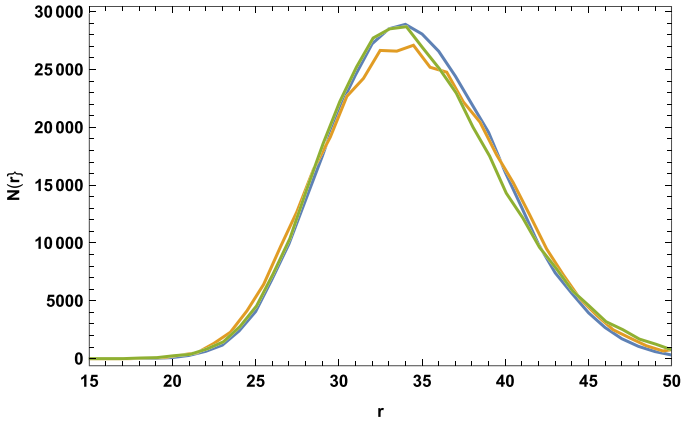

Fig. 11. Distributions of loop distances for loops with winding numbers {1, 0, 0, 0} (blue), {0, 1, 0, 0} (orange) and {0, 0, 1, 0} (green) shifted in r by a shift of order 1.

R is computationally very time-consuming, therefore we decided to perform measurements for a single well-thermalized configuration with $N^{\{4,1\}}$ =160k (the total number of simplices in this configuration is $N_4 = 370\,724$) and the time periodicity $T = 4$ (in fact this is the same configuration we used in the preceding section). For this configuration we measured loops in all spatial and time directions, restricting the length to be below 55 (in this way we could measure the distribution of loop geodesics to the nearest copies in all directions and additionally some geodesics with more complicated winding characteristics). Although the analysis is based only on one configuration, we expect that distributions will self-average to produce a reasonable estimate for a whole ensemble.

We expect the distributions of lengths of all loops connecting the neighboring cells in x, y and z directions to be approximately the same, up to a possible small shift in the length r. This is indeed what is observed. The Fig. 11 shows the length distributions of the {1, 0, 0, 0}, {0, 1, 0, 0} and {0, 0, 1, 0} loops superimposed using a shift of order smaller than 1. The match is not perfect, but we should remember that we are using just a single configuration. The need of making small finite shifts reflects the fact that during the thermalization process the shape of the elementary cell is deformed from the regular symmetric shape it had in the initial hypercube.

Comparing the loop distance in two different directions (Fig. 11), we find that not only is the shape of the distributions similar. In fact loop distances for *all simplices* are highly correlated, which can be seen in the Fig. 12, which presents the correlation between the loop distance in the {1, 0, 0, 0} and {0, 0, 1, 0} directions.

For all simplices in the configuration we assigned a set of numbers measuring distances to their copies in the neighboring cells. These numbers contain interesting information about the internal geometry of the manifold.

- In each direction we find a finite number of loops with the minimal length r_{min}. The minimal loops follow the deepest *valleys* being surrounded by *mountains* which we can view as large volume fluctuations. In some sense, the minimal loops are dual to the minimal boundaries discussed in previous sections.
- The simplices located on the *mountains* (i.e., inside the large volume fluctuations) are characterized by longer loop distances to the neighboring cells. Given a simplex, we can compare

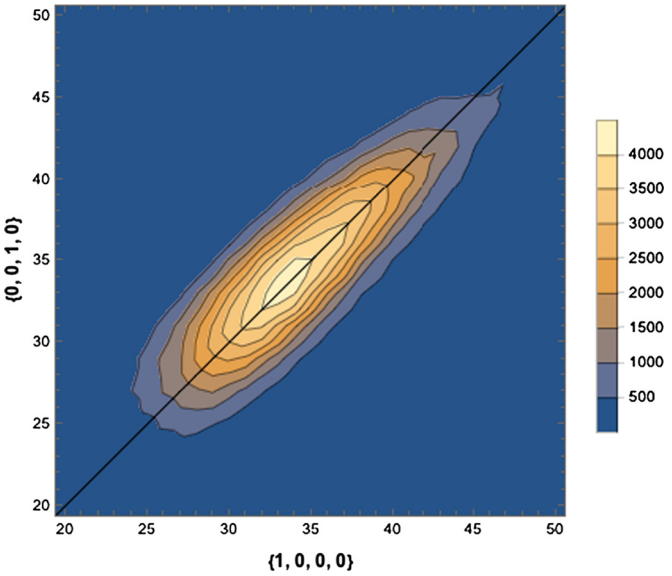

Fig. 12. Correlation between loop distances for loops with winding numbers {1, 0, 0, 0} and {0, 0, 1, 0}.

its loop distance in each direction with the loop distances of its five neighbors. For all simplices with the same loop distance r, we find that the neighboring simplices are characterized by loop distances in the range r, $r \pm 1$ and $r \pm 2$.

- Only for the few shortest loops can we follow a simple path connecting the simplex to its copy that would go through a sequence of neighboring simplices characterized by the *same* value of the loop distance r.
- For longer loops all paths to a copy pass through fragments of loops with smaller loop distances.
- We deduce that the difference between the loop distance r for a particular simplex and the minimal distance r_{min} indicates how far a given simplex is from the minimal loop.

Finally, we will compare the distribution of loop distances for simplices in the fundamental cell in, say, the {0, 0, 1, 0} direction to the distribution of the quantity $L_z = \mathbf{z} + \mathbf{z}'$ discussed earlier. We recall that this quantity is the sum of the distances from a simplex to the two cell boundaries *orthogonal* to the $\mathbf{z}$ direction. We find that the two distributions are highly correlated. An example of this correlation can be seen on the contour plot shown in the Fig. 13.

6. Loop distances in other directions

The universality of the loop distance distribution can be extended to include loops with higher non-trivial winding numbers. The interpretation is that the blob-like structure (valleys and mountains) reflects the fractal structure of the fluctuations of geometry in the model and therefore can be expected to be independent of the direction in which we measure the loop distance distribution. For different directions we expect different minimal loop lengths, and as a consequence of comparing distributions with different argument range we may have to adjust this range to obtain a proper overlap when we compare the distributions. In Fig. 14 we show the comparison of distri-

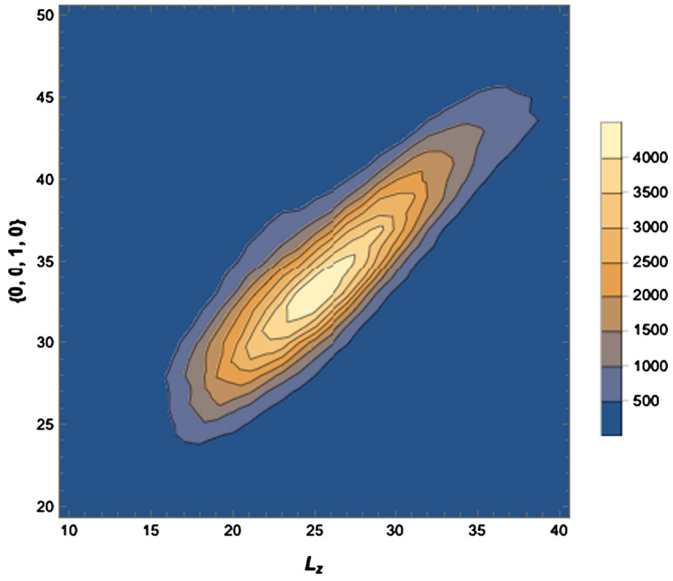

Fig. 13. Correlation of a distribution of L_z (horizontal axis) with a loop distance in $\{0,\ 0,\ 1,\ 0\}$ direction.

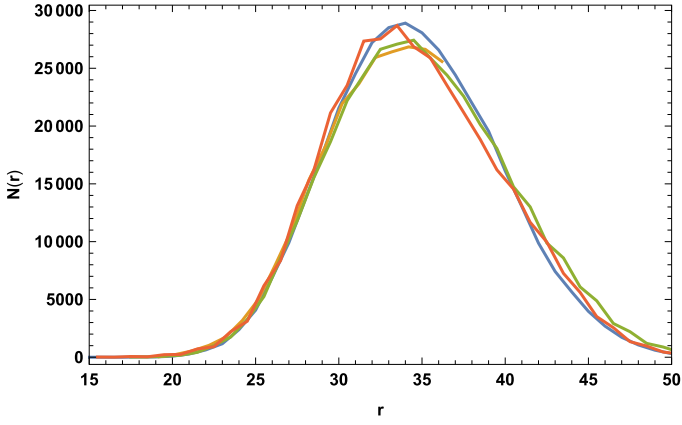

Fig. 14. Distributions of (shifted) loop distances in directions $\{1,\ 0,\ 0,\ 0\}$ (blue), $\{1,\ -1,\ 0,\ 0\}$ (red), $\{1,\ -1,\ 1,\ 0\}$ (green) and $\{1,\ 1,\ 1,\ 0\}$ (orange) showing the universal blob structure.

butions for loop distances in directions $\{1,\ 0,\ 0,\ 0\}$ (blue), $\{1,\ -1,\ 0,\ 0\}$ (red), $\{1,\ -1,\ 1,\ 0\}$ (green) and $\{1,\ 1,\ 1,\ 0\}$ (orange). The last one is seen only as a fragment of a distribution, as it requires a shift of 15 units, and is not contained fully in the region $R < 55$ we analyzed. The universality of the distributions, independent of directions, strongly suggests that the distribution of volume fluctuations is spherically symmetric. At the same time, the difference in the minimal loop distance in different directions most likely reflects that the shape of the elementary cell of our thermalized configuration is non-trivial.

The thermalized configuration discussed here has the four-dimensional topology of T^4. In the time direction there is a foliation, which is absent in spatial directions. Although the periodicity in the time direction is trivial, this does not necessarily mean that the distribution of the loop

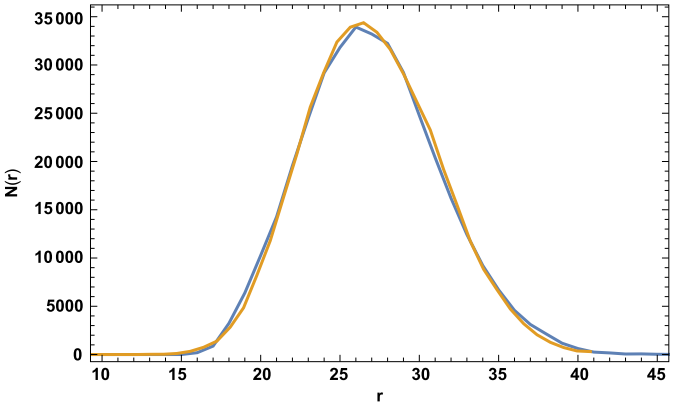

Fig. 15. The loop distance distribution in the time direction, compared to that in the **x** direction.

distances in the time direction $\{0,\ 0,\ 0,\ 1\}$ will be a Dirac delta function. In fact, due to the large spatial volume fluctuations, it has a shape very similar to that in spatial directions. Below, in the Fig. 15, we show the distribution of the loop distances in the time direction ($\{0,\ 0,\ 0,\ 1\}$) (blue) as compared to a shifted and rescaled distribution in the $\{1,\ 0,\ 0,\ 0\}$ direction (orange). The scaling factor used was 1.19.

This result indicates that although we have a foliation in time, the information encoded in the loop distance in spatial and time directions is very similar. The average length of the loop distance in the time direction is expected to depend on the time period T.

7. Conclusion

CDT is a non-perturbative quantum gravity model. It is a model with a build-in cut-off, the length a of the links in the triangulations. In order to prove that it is an interesting model of quantum gravity one has to be able to remove the cut-off in a controlled way and show that the resulting theory satisfies the criteria suitable for a theory of quantum gravity.[7] Two such criteria often mentioned are background independence and diffeomorphism invariance. CDT partially satisfies these criteria already at the regularized level when the cut-off a is non-zero. It is background independent in the sense that it is defined as a sum over a certain class of piecewise linear geometries, and each geometry is given the same weight, except for the weight associated with the Hilbert-Einstein action. However, more remarkable is the fact that the path integral is carried out explicitly as a sum over geometries. The analogy in a gauge theory would be performing the path integral directly over the set of gauge equivalent field configurations. This possibility comes about because we regularize our path integral by using a certain class of piecewise linear geometries, and, as emphasized by Regge [3], one does not need coordinates in order to describe the geometry of piecewise linear geometries. In this sense, not having coordinates is very good and in some sense consistent with a central point in general relativity, where physics is invariant under coordinate transformations. However, coordinates can be very useful, in particular the *right* coordinates, for the description of a certain physical phenomenon. In [6] we showed that using a proper-time coordinate the "quantum universe" observed in the computer simula-

[7] A discussion of how the CDT cut-off can in principle be removed while physics is kept constant can be found in [9].

tions where space had the topology of S^3 could be described by a semi-classical effective action. However, we also encountered the problem that it was difficult to extend the effective action to include space coordinates. Our representation was simply too "diffeomorphism invariant". If the topology of space is that of T^3, the situation is somewhat better. As we have described above, one has the possibility to use the periodic nature of T^3 to construct a kind of pseudo-Cartesian spatial coordinate system. Its status is however somewhat different from the way a coordinate system usually appears in a quantum gravity calculation where the geometry is described in terms of $g_{\mu\nu}(x, y, z, t)$, with x, y, z, t referring to a given coordinate system, the same for any $g_{\mu\nu}(x, y, z, t)$ which appear in the path integral. In our case, we are in principle adjusting our coordinate system to the geometry. The usefulness of such a construction will depend on the nature of the quantum system. If the quantum system is dominated by one kind of configurations, on top of which there are "not-too-wild" quantum fluctuations, this construction can be very useful, in particular if the dominating configuration is not a simple classical or semiclassical configuration. This is seemingly the situation we meet in the de Sitter phase of our quantum gravity model. Certain aspects of the dominating configurations have a semiclassical interpretation in the sense that their features can be described by a suitable time coordinate and an *effective* action depending on the time coordinate. But this action is far from any $\hbar$ expansion used in the path integral and thus far from an expansion related to solutions of the classical action. For such an *effective* action it is *a priori* not clear how to choose a good coordinate system. For this reason we have chosen the "dynamical" approach described above, where the fundamental cell of T^3 is chosen to be as regular as possible for a given configuration. In terms of the "pseudo-Cartesian" coordinates associated with the chosen cell, we observe an interesting spatial structure: a "trunk" of connected four-simplices for each spatial direction, decorated by quantum outgrowths. This suggests a "semiclassical" interpretation even of a spatial section of the four-dimensional universe, which is not so different from the situation in two-dimensional Euclidean quantum gravity, where a typical configuration, when sliced appropriately (choosing the appropriate coordinates for the configuration in question), can be viewed as a main universe dressed with quantum outgrowths (baby universes) [10]. In the case of two-dimensional Euclidean quantum gravity, this slicing and its associated fractal structure determines most aspects of two-dimensional Euclidean quantum gravity. Our preliminary analysis (only based on one large configuration) suggests that the fractal structure of the three-dimensional configurations is less fractal (i.e., more "semiclassical") than in the two-dimensional case, in the sense that there are fewer outgrowths, and they carry less volume than in two-dimensional quantum gravity. Clearly, the precise determination of the fractal structure of the three-dimensional quantum space, such as the determination of critical exponents associated with this structure, requires considerably longer Monte Carlo simulations. However, the less fractal structure also increases the hope that in this way one can obtain a more complete semiclassical effective action expressed in terms of the proper time and these new spatial coordinates.

The use of toroidal topology also allowed us to use loops with non-trivial winding numbers to extract information about the fractal structure of our spatial geometries. This has been done successfully in two-dimensional Euclidean quantum gravity [11], and also here in the four-dimensional case it provides us with a lot of information. In some sense, the shortest non-contractible loops can be considered as dual to the minimal cell boundaries and, like in the two-dimensional case, the shortest loops lie in narrow "valleys", where the surrounding "hills" look like (topologically) spherical outgrowths. Again, further computer simulations should allow one to determine the fractal structure related to "valleys" and "hills", much in the spirit of two-dimensional Euclidean quantum gravity.

Acknowledgements

JA wishes to acknowledge support from the Danish Research Council under grant "Quantum Geometry" (Danmarks Frie Forskningsfond, grant number: 7014-00066B). JGS wishes to acknowledge support of the grant UMO-2016/23/D/ST2/00289 from the National Science Centre, Poland. ZD acknowledges a support of the PhD project "Kartezjusz". AG acknowledges support by the National Science Centre, Poland under grant 2015/17/D/ST2/03479.

References

[1] J. Ambjorn, J. Gizbert-Studnicki, A. Görlich, J. Jurkiewicz, D. Németh, The phase structure of Causal Dynamical Triangulations with toroidal spatial topology, J. High Energy Phys. 1806 (2018) 111, arXiv:1802.10434 [hp-th].

[2] J. Ambjorn, A. Görlich, J. Jurkiewicz, R. Loll, Nonperturbative quantum gravity, Phys. Rep. 519 (2012) 127–210, arXiv:1203.3591 [hep-th].

[3] T. Regge, General relativity without coordinates, Nuovo Cimento 19 (1961) 558.

[4] J. Ambjorn, R. Loll, Nonperturbative Lorentzian quantum gravity, causality and topology change, Nucl. Phys. B 536 (1998) 407, arXiv:hep-th/9805108;
J. Ambjorn, R. Loll, W. Westra, S. Zohren, Putting a cap on causality violations in CDT, J. High Energy Phys. 0712 (2007) 017, arXiv:0709.2784 [gr-qc];
J. Ambjorn, R. Loll, Y. Watabiki, W. Westra, S. Zohren, A string field theory based on causal dynamical triangulations, J. High Energy Phys. 0805 (2008) 032, arXiv:0802.0719 [hep-th].

[5] J. Ambjorn, J. Jurkiewicz, R. Loll, G. Vernizzi, Lorentzian 3-D gravity with wormholes via matrix models, J. High Energy Phys. 0109 (2001) 022, arXiv:hep-th/0106082;
J. Ambjorn, J. Jurkiewicz, R. Loll, G. Vernizzi, 3-D Lorentzian quantum gravity from the asymmetric ABAB matrix model, Acta Phys. Pol. B 34 (2003) 4667, arXiv:hep-th/0311072;
J. Ambjorn, J. Jurkiewicz, R. Loll, Renormalization of 3-d quantum gravity from matrix models, Phys. Lett. B 581 (2004) 255, arXiv:hep-th/0307263.

[6] J. Ambjorn, J. Jurkiewicz, R. Loll, Emergence of a 4-D world from causal quantum gravity, Phys. Rev. Lett. 93 (2004) 131301, arXiv:hep-th/0404156;
J. Ambjorn, J. Jurkiewicz, R. Loll, Reconstructing the universe, Phys. Rev. D 72 (2005) 064014, arXiv:hep-th/0505154;
J. Ambjorn, A. Gorlich, J. Jurkiewicz, R. Loll, Planckian birth of the quantum de Sitter universe, Phys. Rev. Lett. 100 (2008) 091304, arXiv:0712.2485 [hep-th], Phys. Rev. D 78 (2008) 063544, arXiv:0807.4481 [hep-th].

[7] J. Ambjorn, Z. Drogosz, J. Gizbert-Studnicki, A. Görlich, J. Jurkiewicz, D. Németh, Impact of topology in causal dynamical triangulations quantum gravity, Phys. Rev. D 94 (2016) 044010, arXiv:1604.08786 [hep-th];
J. Ambjorn, J. Gizbert-Studnicki, A. Görlich, K. Grosvenor, J. Jurkiewicz, Four-dimensional CDT with toroidal topology, Nucl. Phys. B 922 (2017) 226–246, arXiv:1705.07653 [hep-th].

[8] P.S. Mara, Triangulations for the cube, J. Comb. Theory 20 (1976) 170.

[9] J. Ambjorn, A. Görlich, J. Jurkiewicz, A. Kreienbuehl, R. Loll, Renormalization group flow in CDT, Class. Quantum Gravity 31 (2014) 165003, arXiv:1405.4585 [hep-th].

[10] H. Kawai, N. Kawamoto, T. Mogami, Y. Watabiki, Transfer matrix formalism for two-dimensional quantum gravity and fractal structures of space-time, Phys. Lett. B 306 (1993) 19, arXiv:hep-th/9302133.

[11] J. Ambjørn, T. Budd, The toroidal Hausdorff dimension of 2d Euclidean quantum gravity, Phys. Lett. B 724 (2013) 328, arXiv:1305.3674 [hep-th];
J. Ambjørn, T. Budd, Semi-classical dynamical triangulations, Phys. Lett. B 718 (2012) 200, arXiv:1209.6031 [hep-th];
J. Ambjorn, J. Barkley, T.G. Budd, Roaming moduli space using dynamical triangulations, Nucl. Phys. B 858 (2012) 267, arXiv:1110.4649 [hep-th];
J. Ambjorn, J. Barkley, T. Budd, R. Loll, Baby universes revisited, Phys. Lett. B 706 (2011) 86, arXiv:1110.3998 [hep-th].